Supporting Information

for *Adv. Funct. Mater.,* DOI: 10.1002/adfm.201904668

Irradiation of Transition Metal Dichalcogenides Using a Focused Ion Beam: Controlled Single-Atom Defect Creation

*Jothi Priyanka Thiruraman, Paul Masih Das, and Marija Drndic´**

Supporting Information

Irradiation of Transition Metal Dichalcogenides using a Focused Ion Beam: Controlled Single-Atom Defect Creation

Jothi Priyanka Thiruraman[†], *Paul Masih Das*[†], *Marija Drndić**

[†]These authors contributed equally to this work.

Jothi Priyanka Thiruraman[1,2], Paul Masih Das[1], Prof. Marija Drndić[1]

[1]Department of Physics and Astronomy, University of Pennsylvania, Philadelphia, Pennsylvania 19104, USA.

[2]Department of Electrical and Systems Engineering, University of Pennsylvania, Philadelphia, Pennsylvania 19104, USA.

*E-mail: drndic@physics.upenn.edu.

Keywords: ion beam irradiation, 2D materials, defects, nanopores, transition metal dichalcogenides

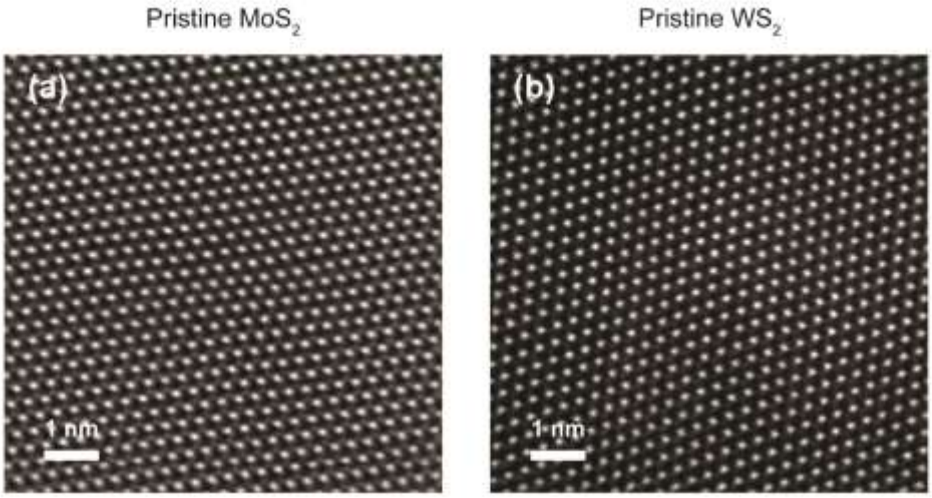

Figure S1. HAADF AC-STEM images of pristine CVD-grown monolayer (a) MoS_2 and (b) WS_2 taken at 80 kV. Bright spots correspond to transition metal (Mo, W) atoms in a trigonal prismatic (2H) coordination with chalcogen (S) atoms.

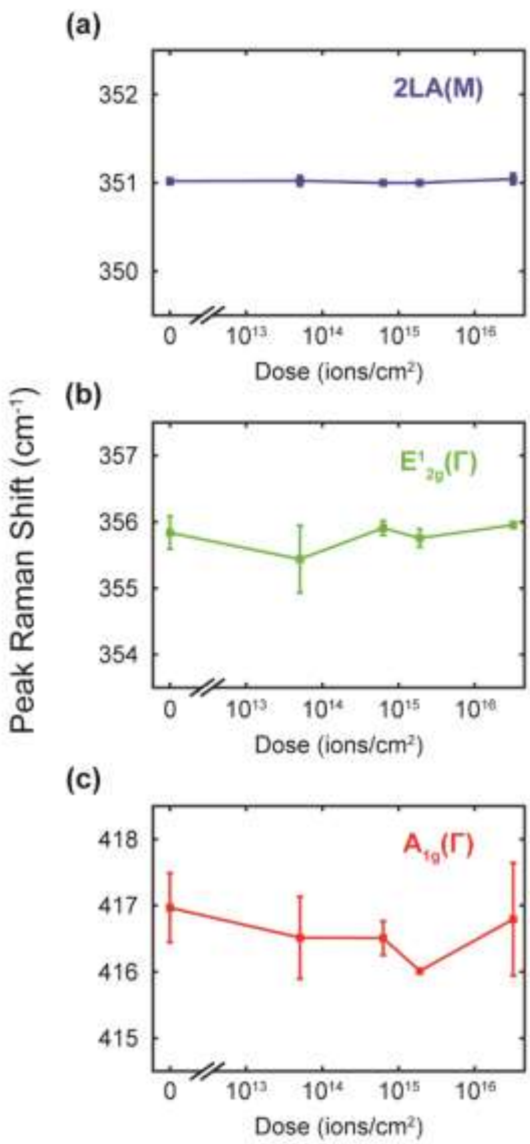

Figure S2. Raman peak shifts for suspended monolayer WS_2 exposed to FIB irradiation with doses between 0 and 10^{17} ions/cm^2. Raman spectra (shown in Figure 2) were fit to three phonon modes: (a) second-order longitudinal acoustic 2LA(M), (b) in-plane $E^1_{2g}(\Gamma)$, and (c) out-of-plane $A_{1g}(\Gamma)$ (see Experimental Section). No discernible peak shifts above the spectrometer resolution (0.5 cm^{-1}) were observed over the dose range studied here.

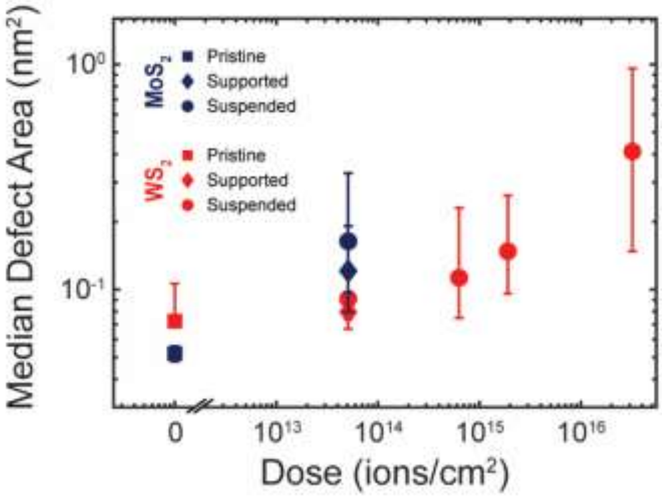

Figure S3. Median defect area for (blue) MoS_2 and (red) WS_2 as a function of FIB irradiation dose. Pristine, substrate-supported, and suspended systems are represented by squares, diamonds, and circles, respectively. Error bars represent two quartiles above and below the median. Similar to defect density and average defect area (see Figure 4), median defect areas are larger (i) at higher irradiation doses, (ii) in suspended systems, and (iii) in MoS_2 (compared to WS_2).

Sample Type	FIB Exposure Dose ($ions/cm^2$)	AC-STEM Imaged Area (nm^2)
Pristine MoS_2	0	1.56×10^3
Substrate-Supported MoS_2	5.1×10^{13}	3.56×10^3
Suspended MoS_2	5.1×10^{13}	1.66×10^4
Pristine WS_2	0	2.47×10^3
Substrate-Supported WS_2	5.1×10^{13}	4.07×10^3
Suspended WS_2	5.1×10^{13}	1.69×10^4
Suspended WS_2	6.4×10^{14}	2.29×10^4
Suspended WS_2	1.9×10^{15}	4.28×10^4
Suspended WS_2	3.1×10^{16}	2.94×10^4

Table S4. Total imaged area of atomic resolution HAADF AC-STEM micrographs used to calculate defect density, average defect area, and median defect size for various suspended and substrate-supported TMDs. A description of the analysis procedure can be found in the Experimental Section. Defect histograms for each listed sample are shown in Figures S5-6 while summarized results are given in Figures 4 and S3.

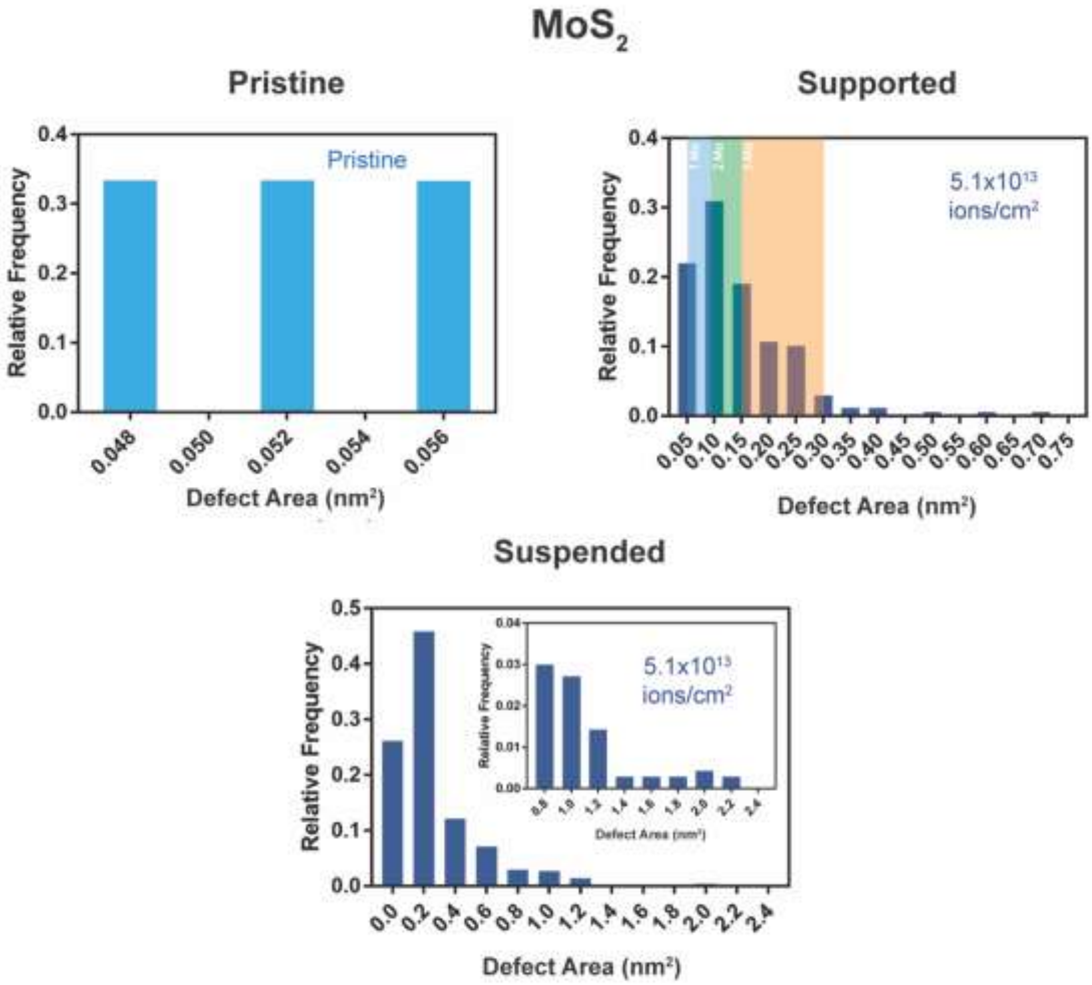

Figure S5. Histograms of individual defects for MoS_2 under several irradiation conditions (see Figure 4) showing relative frequency of defect occurrence (sum normalized to one) as a function of defect area. Only defects above the size of a single transition metal atom (area > 0.05 nm^2) are included due to AC-STEM resolution and contrast limits. Light blue, green and orange shading indicate the 1Mo, 2Mo and 3Mo defect types respectively. The inset in the bottom row is a zoom in of the larger defect area regime, showing a small proportion of somewhat larger defects (up to ~2.2 nm^2).

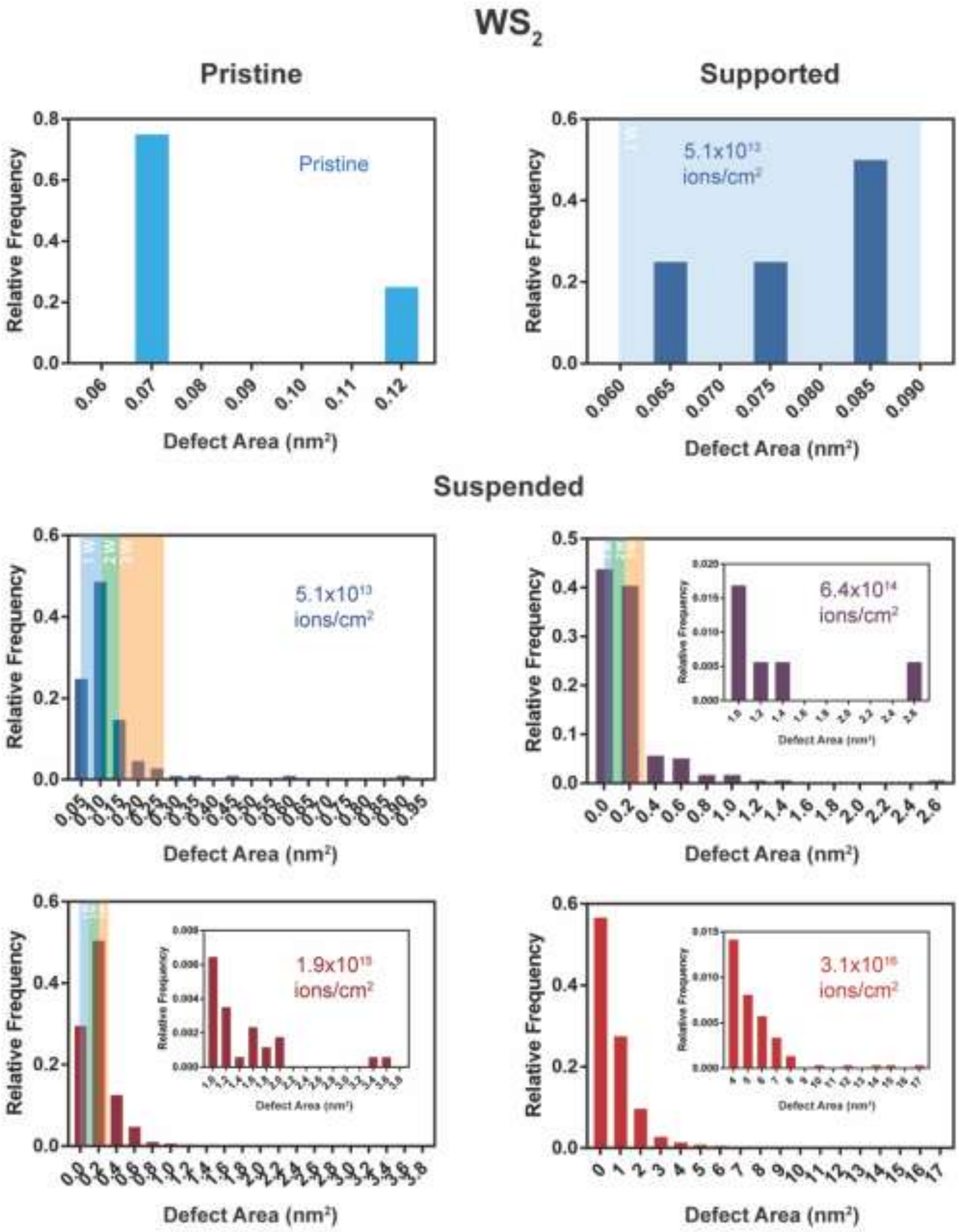

Figure S6. Histograms of individual defects for WS_2 under several irradiation doses (see Figure 3) and substrate conditions (see Figure 4) showing relative frequency of defect occurrence (sum normalized to one) as a function of defect area. Only defects above the size of a single transition metal atom (area > 0.05 nm^2) are included due to AC-STEM resolution and contrast limits. Light blue, green and orange shading indicate the 1W, 2W and 3W defect types respectively (as shown in Figure 5). The insets in the middle and bottom rows are zoom ins for the larger defect area regime, showing a small contribution of larger defects up to ~ 17 nm^2.

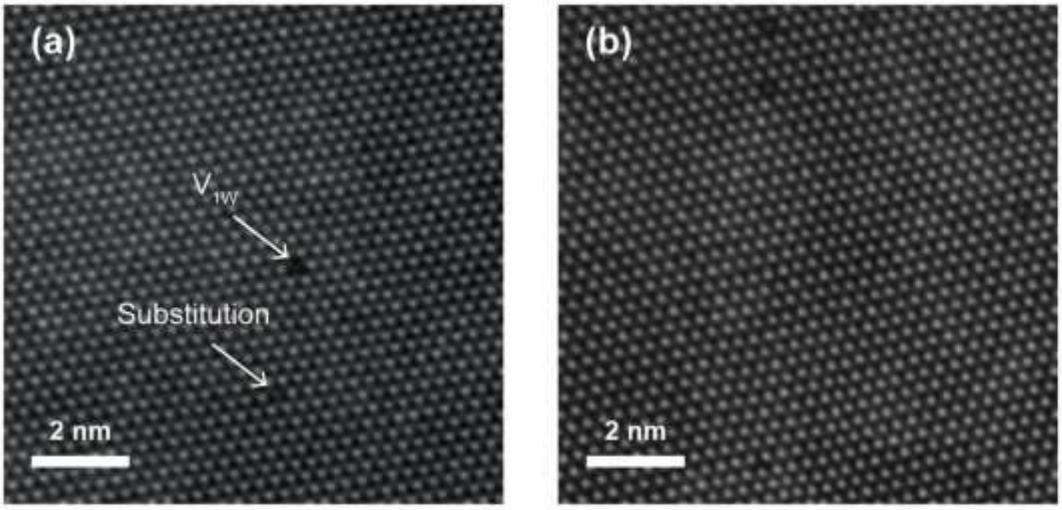

Figure S7. AC-STEM images of substitutional dopants from (a) suspended WS_2 exposed to 6.4×10^{14} ions/cm^2 and (b) substrate-supported WS_2 exposed to 5.1×10^{13} ions/cm^2. Substitutions are primarily observed in samples at low irradiation doses (10^{13}-10^{14} ions/cm^2) and are not seen in pristine MoS_2 and WS_2 (Figure S1).

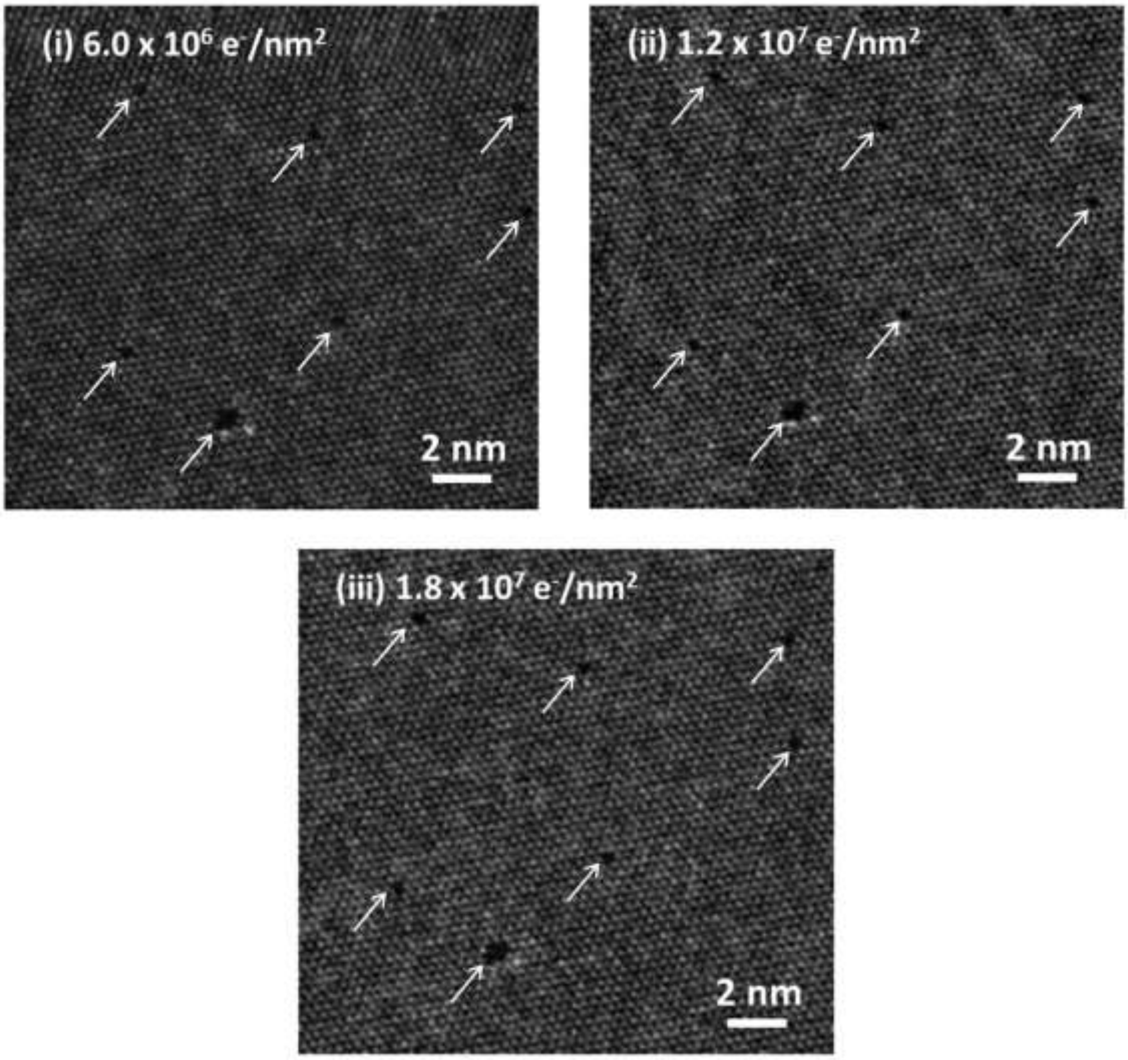

Figure S8. AC-STEM micrographs of FIB-irradiated (6.4×10^{14} ions/cm^2) monolayer WS_2 under constant imaging conditions (*i.e.,* STEM raster scanning). Under electron doses of (i) 6.0×10^6 (1 scan), (ii) 1.2×10^7 (2 scans), and (iii) 1.8×10^7 e$^-$/nm^2 (3 scans), existing defects (white arrows) did not expand or migrate, suggesting negligible electron beam-induced radiation damage during imaging. This study utilizes an acceleration voltage of 80 kV, STEM probe current of 22 pA, and imaging doses of ~ 10^6 e$^-$/nm^2 (see Methods), which does not cause knock-on damage in monolayer TMDs.[12,28]

Sample Type	***Equation (1):*** $D = \frac{It}{qA}$ (ions/cm^2)	***Equation (2):*** $D = \frac{I\, t_d N_s}{qA_{beam}}$ (ions/cm^2)	**Defect Density** (sites/cm^2)
Pristine MoS_2	0	0	1.1×10^{11}
Substrate-Supported MoS_2	1.1×10^{12}	5.1×10^{13}	7.9×10^{12}
Suspended MoS_2	1.1×10^{12}	5.1×10^{13}	1.4×10^{13}
Pristine WS_2	0	0	1.5×10^{11}
Substrate-Supported WS_2	1.1×10^{12}	5.1×10^{13}	8.6×10^{10}
Suspended WS_2	1.1×10^{12}	5.1×10^{13}	9.0×10^{11}
Suspended WS_2	1.4×10^{13}	6.4×10^{14}	1.9×10^{12}
Suspended WS_2	4.2×10^{13}	1.9×10^{15}	9.9×10^{12}
Suspended WS_2	7.0×10^{14}	3.1×10^{16}	9.3×10^{13}

Table S9. FIB irradiation dose calculations (columns 2-3) and defect densities (column 4) for pristine, suspended, and substrate-supported TMDs. As discussed in the main text, calculations using equation (1) are inaccurate for 2D materials and result in ion dose values an order of magnitude lower than defect densities (for example, see Suspended MoS_2). Equation (2) provides a more accurate dose estimate.